

Microstructure-Strength Properties in Ceramics: I, Effect of Crack Size on Toughness

ROBERT F. COOK,^{*,#} BRIAN R. LAWN,^{*} and CAROLYN J. FAIRBANKS^{*}

Center for Materials Science, National Bureau of Standards, Gaithersburg, Maryland 20899

A systematic study of the inert-strength characteristics of ceramics as a function of crack size relative to grain size has been made using controlled indentation flaws. The focus of the test program is on aluminas, with barium titanates and glass-ceramics providing support data in confirmation of general trends. On progressively diminishing the indentation load, the strengths first show a steady increase, but subsequently tend to a plateau, as the contact size begins to approach the characteristic grain size. A simple extension of conventional indentation fracture mechanics theory (incorporating residual contact stresses) is developed to describe this scale transition. The basis of the analysis is the postulated existence of a "microstructural driving force," grain-localized at the center of the pennylike radial crack, in direct analogy to the indentation driving force. This description provides closed-form solutions to the fracture mechanics equations, such that the data are interpretable in terms of an apparent *R*-curve function. Only two quantities are required to specify the function completely, one relating to the macroscopic toughness determined from large-scale crack specimens and the other to a microstructure-associated stress intensity factor. These quantities are advocated as useful reliability parameters. It is found that the second quantity can vary widely from material to material, even within a given class, to the extent that materials which show superior strength characteristics at large indentation loads may be dramatically weaker at low loads. The indications are that, at least for aluminas, the key to such weakening effects is to be found in the grain-boundary structures. The study emphasizes the need for extreme caution in extrapolating macroscopic-crack data unconditionally into the microscopic-flaw region, and for more fundamental investigations into the underlying physical processes actually responsible for the microstructural driving forces.

I. Introduction

MODERN-DAY theories of the strength of ceramics rely heavily on the precepts of fracture mechanics—in particular, that the flaws responsible for failure have the character of well-defined cracks in elastic continua. It is therefore implicit that the "laws" we use to describe fracture processes, most notably those involving toughness (equilibrium fracture) and crack velocity (nonequilibrium fracture) parameters, are continuum based. Such a descriptive basis would appear to be perfectly justifiable in the case of glasses and fine-grained polycrystals where the scale of the typical fracture event greatly exceeds that of the material microstructure. The question arises as to the applicability of these fracture mechanics descriptions to ceramics with coarser microstructures, such that the size of the strength-controlling flaws is of the same order as the grains themselves. Is it valid to extrapolate from toughness and crack velocity test data on large-scale crack specimens to this microscopic-flaw region?

There is now considerable evidence, particularly from the fractographic studies of Rice and co-workers, to suggest that micro-

structure can indeed be an important factor in characterizing the strength of ceramics.¹⁻¹⁴ Generally, there is a tendency for the strength to be somewhat smaller than one would expect from macroscopic toughness values as the measured flaw size gets smaller. The prevailing interpretation of this tendency is that the material toughness must increase in some systematic manner with crack size, in direct analogy to the *R*-curve effects reported in other, crack propagation configurations: at the lower end of the crack-size spectrum the toughness is determined by single-crystal cleavage energies (transgranular fracture) or grain-boundary energies (intergranular fracture); at large crack sizes the microstructural influence is "averaged out," and the toughness becomes representative of the polycrystalline aggregate.

Thus far there has been little serious effort to provide a detailed analysis of the crack/microstructure size dependence of toughness for incorporation into a strength formulation. Evans *et al.*^{15,16} constructed empirical toughness functions which do indeed account for the *R*-curve phenomenology, but made no attempt to justify their functions in terms of actual strength data. Rice and Lewis¹⁴ suggest that these functions are not fully consistent with the strength data that are available. The lack of consensus here simply reflects the fact that conventional strength testing, relating as it does to the characteristics of naturally occurring (e.g., machining or processing) flaws, does not possess the necessary element of experimental control for definitive evaluation of crack-size dependencies in the failure mechanics. There is, for instance, the contentious issue as to whether small-scale flaws fail spontaneously from their initial configuration^{5,6} or undergo a stage of stable (equilibrium) growth prior to instability.^{15,16} It is clear that unless we can contrive our flaw population in such a way that the location of the critical member may be predetermined, thereby allowing for direct observation of the response to the applied stresses, such issues will not be easily resolved.

Our way of controlling the fracture origin is to introduce indentation flaws into the prospective strength specimens. The associated crack patterns are geometrically well-defined and, despite the presence of residual contact stress fields, are amenable to rigorous fracture mechanics analysis at all stages of their evolution.¹⁷⁻²¹ Most important, the size of the cracks can be varied systematically via the contact load, thereby allowing for controlled progression from macroscopic to microscopic domains. It has been demonstrated that the simple inverse relations between strength and contact load derived on the basis of a continuous solid structure hold well for relatively homogeneous materials, e.g., silicate glasses, over a large range of flaw sizes.^{18,22} Since the proportionality terms in these relations strongly involve the material toughness,^{18,23} it may be expected that microstructural effects should show up as systematic departures from ideal behavior in the low-load region. Such departures have indeed been reported in two recent studies, on alumina²⁴ and glass-ceramic²⁵ materials. It is the need for a detailed fracture mechanics formulation of these potentially important influences on strength properties (particularly in the context of design) which provides the primary motivation for the work to be described here.

Accordingly, we shall use the indentation technique to investigate the microscopic-to-macroscopic crack-size transition in "coarse-grained" ceramics. The presentation will be in two parts. Part I will deal with the manifestations of this transition in toughness properties, and Part II similarly in fatigue properties. Alumina will constitute our "model" ceramic for the bulk of the experimental study, but results will also be presented on barium titanate and glass-ceramic materials to demonstrate the generality of the

Received February 28, 1985; revised copy received July 29, 1985; approved August 9, 1985.

Supported by the U.S. Air Force Office of Scientific Research. Support for R. F. Cook provided by the NBS Guest Worker Program.

^{*}Member, the American Ceramic Society.

[#]Present address: I.B.M., T. J. Watson Research Center, Yorktown Heights, NY 10598.

procedure. The data trends will be shown to be consistent with a simple *R*-curve function based on the notion of a "grain-localized" crack driving force.²⁴ It will be seen that the microstructural influence can be dramatic, both in the reduction in the apparent toughness in the microscopic region and in the range of crack sizes (relative to some characteristic microstructural dimension) over which this influence persists.

One aspect of the microstructural problem which will *not* be addressed explicitly here is the *underlying cause* of the crack-size transition. Various possible contributing factors have been discussed in the literature,¹⁴ including crack pinning, deflection and branching, the initiation and coalescence of microcracks, and the generation of internal stress fields (e.g., due to thermal expansion or elastic anisotropy). It is self-evident that a fundamental description of crack-size effects ultimately rests with a proper understanding of these factors. Currently, this understanding is almost totally lacking; definitive experiments to determine which contributions dominate in specific material types do not abound in the ceramics literature. The virtue of the fracture mechanics analysis to be developed in this study is that, provided we are content with a phenomenological account of the toughness properties, we can set up a theoretical framework without any knowledge of physical processes whatever. By independently developing an engineering formalism for the crack-size transition we can hope to provide a sound basis for reliability evaluation and, at the same time, to establish a rationale for the future study of specific microstructural mechanisms.

II. Fracture Mechanics Model

The starting point in the fracture mechanics analysis is the stress intensity factor for a pennylike indentation crack of characteristic radial dimension c produced at a peak contact load P and subsequently subjected to an applied tensile stress σ_a (Fig. 1). Our objective is to modify the conventional formulation^{18,20,26} in such a way as to allow for an increasing contribution as the crack size diminishes in scale relative to some characteristic microstructural dimension d . Accordingly, for equilibrium fracture (pertinent to inert-strength testing conditions) we may write, following Ref. 24

$$K = K_a + K_r$$

$$= \psi \sigma_a c^{1/2} + \chi P / c^{3/2} = K'_c \quad (1)$$

where ψ and χ are dimensionless crack geometry and elastic-plastic constraint "constants," respectively.[†] The terms K_a and K_r in this expression represent corresponding contributions to the net crack driving force from the applied loading and the residual contact fields. The problem now reduces to one of determining K'_c as an appropriate function of c , with some provision for incorporating (either explicitly or implicitly) the microstructural scaling parameter d .

In determining such a function, we need to satisfy the limiting condition that K'_c should tend to the polycrystalline toughness, K_c^∞ , say, as c becomes large relative to the scale of the microstructure. In accordance with the *R*-curve notion, this function should diminish monotonically as c becomes small. Previously,²⁴ it was argued that the microstructural influence could be considered to be "grain-localized" at the center of the pennylike radial crack, effectively giving rise to a microstructural stress intensity factor K_m , in much the same sense as the indentation influence manifests itself as the residual stress intensity factor K_r in Eq. (1).^{17,19} In terms of this analogy we may write the crack-size dependence of the toughness function in the form

$$K'_c = K_c^\infty - K_m$$

$$= K_c^\infty - \mu Q / c^{3/2} \quad (2)$$

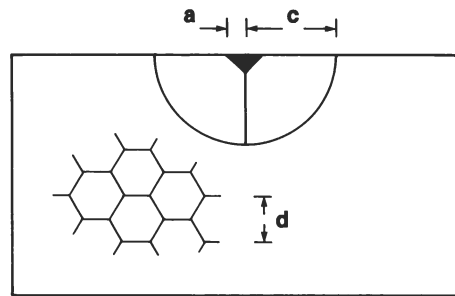


Fig. 1. Schematic of indentation fracture geometry in material with well-defined microstructure. Configuration illustrated is for Vickers pyramid indenter in normal contact (load P), with one of two mutually orthogonal pennylike radial cracks oriented for maximum tension in subsequently applied stress field (stress σ_a). Dimensions a , c , and d characterize scale of central hardness impression, radial crack, and microstructure "grains," respectively. Typically, c is 2 to 3 times a at completion of indentation cycle and extends stably by a further factor of ≈ 2.5 during an inert strength test.

The quantity μQ has the interpretation of a "microstructural driving force," *real or effective*, analogous to χP in the indentation formalism. This implied "equivalence" between indentation and microstructural stress intensity factors has to be seen for what it is—a device for obtaining a working fracture mechanics equation. Our justification for proceeding this way is that Eq. (2) will lead us to closed-form solutions in the strength formulation below. The test of the usefulness of the approach will be in the success with which we can account for the trends in actual strength data.

Equations (1) and (2) may now be combined to give the modified stress intensity factor for equilibrium indentation cracks

$$K = K_a + K_r + K_m$$

$$= \psi \sigma_a c^{1/2} + (\chi P + \mu Q) / c^{3/2} = K_c^\infty \quad (3)$$

It will be seen that this expression has exactly the same crack-size dependence as its unmodified counterpart (cf. Eq. (1)); effectively, all we have done is to replace χP in the old expression by the composite force $\chi P + \mu Q$. Explicit solutions for the strength may now be obtained in the usual way. Thus in the limit of *large* cracks, i.e., $\chi P \gg \mu Q$, we may appeal directly to previous work^{18,26} for the maximum applied stress that the indented specimen can sustain

$$\sigma_m^P = 3K_c^\infty{}^{4/3} / 4^{4/3} \psi (\chi P)^{1/3} \quad (4a)$$

where the superscript P is to denote an "indentation-controlled" region of behavior. The simple inverse relation between strength and contact load alluded to in the Introduction is in evidence in Eq. (4a). Now in the opposite limit of small cracks, i.e., $\chi P \ll \mu Q$, we may proceed by direct inspection to write down a solution of identical form

$$\sigma_m^Q = 3K_c^\infty{}^{4/3} / 4^{4/3} \psi (\mu Q)^{1/3} \quad (4b)$$

with the superscript Q denoting a "microstructure-controlled" region. The important difference in this second limiting solution is that the strength is no longer dependent on load. Figure 2 shows Eqs. (4a) and (4b) as straight lines in (logarithmic) $\sigma_m(P)$ coordinates. The intersection point at $P = P^*$ in this plot conveniently delineates the two regions of behavior. We may note that by equating σ_m^P and σ_m^Q we obtain

$$\chi P^* = \mu Q \quad (5)$$

which offers the prospect of "calibrating" the unknown microstructural driving force parameters in terms of measurable values of P^* .

[†]These "constants" may not be material independent. In particular, it can be shown that $\chi \propto (E/H)^{1/2}$, where E is Young's modulus and H is hardness (Ref. 19).

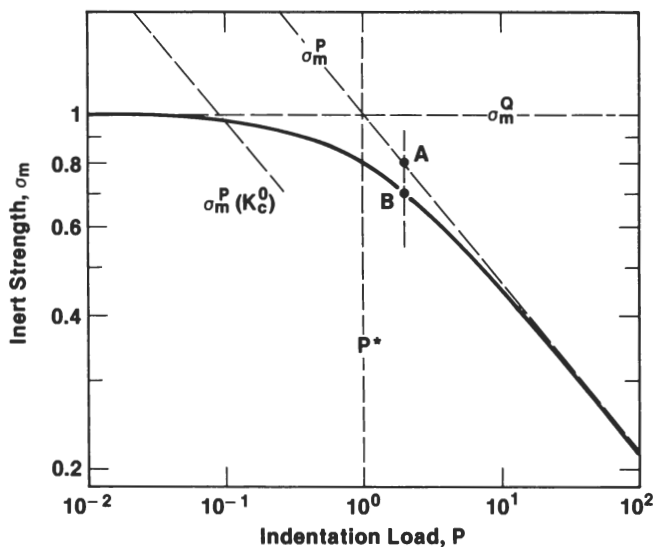


Fig. 2. Normalized plots of strength vs indentation load. Solid curve is general solution (Eq. (8)) and dashed broken lines asymptotic to this curve are limiting solutions (Eqs. (4a) and (4b)). Intersection point between latter two solutions conveniently distinguishes indentation- and microstructure-controlled regions of behavior. Dashed line at left is potential lower-bound solution at small loads, obtained by reevaluating Eq. (4a) with K_c^0 (single-crystal or grain-boundary toughness) in place of K_c^∞ (polycrystalline toughness).

It is instructive at this stage to derive a more general strength-load formalism from Eq. (3), starting from first principles. It is readily seen that $K(c)$ passes through a minimum for any specified P and σ_a . The extremum condition $dK/dc = 0$ therefore defines the crack configuration at which the equilibrium becomes unstable. Applying this condition to Eq. (3) gives, in conjunction with Eq. (5), the critical crack size at instability

$$c_m = [3\chi(P + P^*)/\psi\sigma_m]^{1/2} \\ = [4\chi(P + P^*)/K_c^\infty]^{2/3} \quad (6)$$

where σ_m is the corresponding critical applied stress. In comparison with the initial crack size at $\sigma_a = 0$

$$c_0 = [\chi(P + P^*)/K_c^\infty]^{2/3} \quad (7a)$$

we have $c_m/c_0 = 4^{2/3} = 2.5$, signifying a stable growth stage prior to failure independent of the relative values of P and P^* . We may note a special case of Eq. (7a) at $P = 0$

$$c_0^0 = (\chi P^*/K_c^\infty)^{2/3} \quad (7b)$$

corresponding to the minimum flaw size that the microstructure can apparently sustain. Any flaw nucleus, however small initially, will tend to "pop in" to this value.

Equation (6) may now be solved for the critical stress

$$\sigma_m = 3K_c^\infty/4^{4/3}\psi\chi^{1/3}(P + P^*)^{1/3} \\ = \sigma_m^0 P^{1/3}/(P + P^*)^{1/3} \\ = \sigma_m^0 P^{1/3}/(P + P^*)^{1/3} \quad (8)$$

where we have invoked Eqs. (4) and (5). The second and third forms of this result are useful for demonstrating the manner in which the function $\sigma_m(P)$ asymptotically approaches the limiting cases considered earlier. A plot of this general function is included in Fig. 2. It will be noted from Eq. (8) that of the three measurable material constants σ_m^0 , $\sigma_m^0 P^{1/3}$, and P^* , only two are required to provide a unique determination of the strength characteristics in Fig. 2.

Consider now how this formulation bears on the use of the indentation flaw method to measure toughness.²³ In the idealized

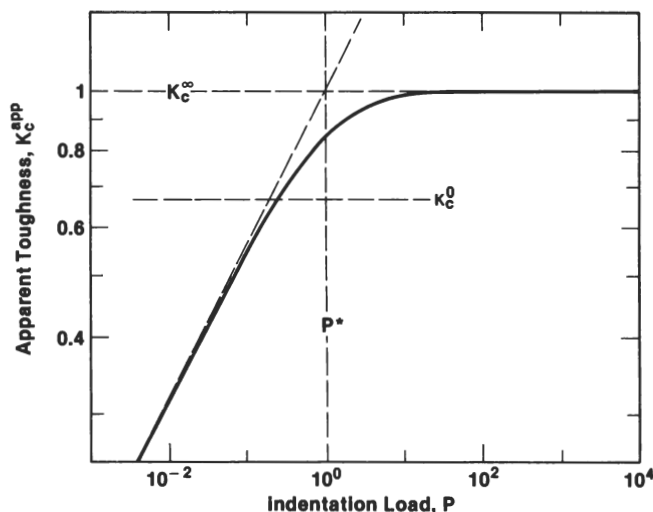


Fig. 3. Normalized plot of apparent toughness vs indentation load (Eq. (10)), showing R -curve behavior. Upper-bound (K_c^∞) and (potential) lower-bound (K_c^0) limits are indicated. Note that P^* uniquely determines "range" of microstructural influence.

theory for homogeneous materials, as represented by Eq. (4a), the toughness may be evaluated from

$$K_c^\infty = (256\psi^3\chi/27)^{1/4}(\sigma_m^0 P^{1/3})^{3/4} \quad (9)$$

When microstructural effects are present, Eq. (9) retains its validity only in the limiting region of large P . Thus, whereas experimentally we measure a value σ_m at given load P , e.g., at point B in Fig. 2, Eq. (9) relates theoretically to the corresponding value along the asymptotic σ_m^0 line, i.e., point A . It is clear from Fig. 2 that the deviation between points A and B becomes greater as the test load diminishes, so the potential discrepancy in toughness evaluations takes on increasingly significant proportions as we enter the microstructure-controlled region. Accordingly, taking Eq. (9) in conjunction with Eq. (8), we may define an "apparent" toughness

$$K_c^{app} = K_c^\infty(\sigma_m P^{1/3}/\sigma_m^0 P^{1/3})^{3/4} \\ = K_c^\infty[P/(P + P^*)]^{1/4} \quad (10)$$

A plot of $K_c^{app}(P)$ is given in Fig. 3. Special note may be made of the tendency for K_c^{app} to level out at the polycrystalline toughness K_c^∞ at $P \gg P^*$, and to fall off monotonically in the low-load region $P \ll P^*$. Our description contains the essential ingredients of R -curve behavior. The R -curve, as traditionally defined, expresses the apparent toughness determined from the applied loading as a function of crack size. In terms of Eq. (2), the R -curve function is expressible as the function $K'_c(c)$. The function $K_c^{app}(P)$ in Eq. (10) embodies the same information, but expresses it instead as a function of the more accessible variable P .

An important issue which needs to be addressed here is that of a lower bound for K_c^{app} . There is no provision in Eq. (10) for such a limit; at $P \rightarrow 0$ we have $K_c^{app} \rightarrow 0$. It has been suggested by others that the apparent toughness should not drop below the value appropriate to either single-crystal or grain-boundary fracture, depending on whether the cracking mode is transgranular or intergranular. We indicate such a bound by the cutoff line K_c^0 in Fig. 3. This kind of cutoff would be manifest in the strength plots of Fig. 2 as a transition onto the $\sigma_m^0(K_c^0)$ line at low P .

Thus far the formulation has been developed exclusively in terms of effective point "driving forces" χP and μQ . The advantage here is the accessibility of indentation load as an independent test variable; P can be measured directly and Q can be determined via the transition load P^* . However, there are many who prefer to think in terms of characteristic scaling dimensions, as indicated in

Table I. Specifications for Materials Used in This Study*

Material	Designation	Preparation	Major phase (%)	Microstructure, d (μm)	Specimen dimensions [†] (mm)
Al_2O_3	Sapphire [‡]	Verneuil	100		(D) 25×1
	AD999 [§]	Sintered	99.9	3	(D) 25×2
	AD90 [§]	Sintered	90	4	(D) 25×2
	Vistal (VI1) [§]	Sintered	99.9	20	(D) 25×2
	Vistal (VI2) [§]	Sintered + aged	99.9	25	(D) 25×2
	F99	Hot-pressed	99	6	(B) $40 \times 5.5 \times 4$
	HW	Sintered	99.7	35	(B) $40 \times 5 \times 3$
BaTiO_3	CH ^{**}	Sintered	99	7	(B) $25 \times 5 \times 3$
	NRL1 ^{††}	Hot-pressed	99.5	1	(B) $36 \times 5 \times 2.5$
	NRL2 ^{††}	Hot-pressed	99.5	150	(B) $36 \times 5 \times 2.5$
Glass-ceramic	SL1 ^{‡‡}	Heat-treated		17	(B) $25 \times 5.5 \times 3.5$
	SL2 ^{‡‡}	Heat-treated		20	(B) $25 \times 5.5 \times 3.5$
	SL3 ^{‡‡}	Heat-treated		41	(B) $25 \times 5.5 \times 3.5$
	VPI1 ^{§§}	Heat-treated		1.3	(D) 12.5×1
	VPI2 ^{§§}	Heat-treated		1.1	(D) 12.5×1
	VPI3 ^{§§}	Heat-treated		1.6	(D) 12.5×1

*Table includes materials used in other laboratories. [†](D) = disks, (B) = bars. [‡]Adolf Meller Co., Providence, RI. [§]Coors Porcelain Co., Golden, CO. ^{||}Frederichsfeld Co., GmbH, Mannheim, West Germany. ^{||}Haldenwanger Co., West Germany. ^{**}Channel Industries, Santa Barbara, CA. ^{††}Naval Research Laboratories, Washington, DC. ^{‡‡}Sandia Laboratories, Albuquerque, NM (lithia-silicate glass-ceramics; see Ref. 28). ^{§§}Virginia Polytechnic Institute, Blacksburg, VA (cordierite glass-ceramics, from Corning base glass, Corning Glass Works, Corning, NY; see Ref. 25).

Fig. 1: that is, indentation half-diagonal a for the flaw size, grain diameter (or interparticle mean free path, whichever is more appropriate) d for the microstructure size. The requisite connecting relation for the indentation parameters is straightforward

$$P = \alpha H a^2 \quad (11)$$

where H defines the material hardness in terms of the contact pressure and α is a geometrical constant ($\alpha = 2$ for Vickers indenters). The corresponding relation for the microstructural parameters cannot be specified in explicit form without a priori knowledge of underlying mechanisms, in which case we can only write

$$Q = \beta f(d, \dots) \quad (12)$$

with β another geometrical constant. For the special case of geometrically similar processes it can be shown that $Q \propto d^{3/2}$ (so that K_m in Eq. (2) is uniquely determined by the scaling ratio c/d),²⁴ which leads to the classical strength/grain-size relation $\sigma_m^Q \propto d^{-1/2}$ in Eq. (4b).¹⁻³ However, other than to note the inverse dependence here, we shall give no further consideration to the manner in which d enters the general strength formalism.

III. Experimental Procedure

A comprehensive indentation-strength test program was carried out on three groups of ceramic materials: aluminas, barium titanates, and glass-ceramics. These materials are listed in Table I, along with pertinent information on preparation, composition, and scale of microstructure. The aluminas were chosen for specially detailed study, mainly because of their availability in a wide range of microstructural forms, including sapphire. The barium titanates and glass-ceramics were included in the study to examine the generality of the phenomena. These material listings incorporate results from previous investigations in our laboratories^{24,27,28} and by Pohanka at the Naval Research Laboratories^{27,29} (barium titanate) and Hasselman's group at Virginia Polytechnic Institute²⁵ (glass-ceramic). Some of the specimens were conveniently supplied in the form of disks ready for biaxial testing. The others came as plates and were subsequently cut up into bars for uniaxial bend testing. The edges of the latter specimens were rounded in an attempt to minimize spurious failures from handling damage. Most of the materials were tested with their surfaces in the as-fired state; where the presence of surface compressive stresses was suspected

(e.g., due to sawing or machining),³⁰ the specimens were either annealed or polished.

The bulk of the specimens were indented at the centers of their prospective tensile faces with a Vickers diamond pyramid. With the bars, care was taken to orient one set of radial cracks normal to the prospective tensile axis. Some specimens were left unindented as controls. Contact loads used covered the range 0.5 to 300 N, although in most of the materials this range was restricted, at the low end by the tendency for "naturally occurring" flaws to dominate the indentation flaws and at the high end by excessive chipping. All indentations were made in air and were allowed to sit for no more than 30 min before strength testing.

The biaxial strength tests were made using a flat circular punch, thickness 4 mm, on 3-point support, diameter 20 mm.³¹ The uniaxial strength tests were made in 4-point bending, inner span 7 mm and outer span 23.5 or 38 mm (depending on the available lengths of the bars). A drop of silicone oil was placed onto the indentation site prior to breaking, and the failure times kept below 20 ms (using a piezoelectric cell to record the load at fracture³²), to minimize fatigue effects in the results. (It will be recalled from Section II that the assumption of equilibrium conditions in the fracture process requires that the strengths be measured in strictly inert environments.) Strength values were calculated from the breaking loads and specimen dimensions using thin plate³¹ and beam³³ formulas.

Special care was taken to examine all specimens after strength testing to verify the contact site as the origin of failure. At the higher indentation loads the incidence of contact-source failures was almost invariable. At the lower loads the success rate diminished markedly. In such cases the "unsuccessful" tests were simply incorporated into the data pool for the unindented controls. Selective observations were also made on some of the specimens during the testing, particularly on the aluminas, using an inverted microscope fixture.¹⁸ In this manner the critical indentation flaw response could be followed directly during the evolution to final instability. These latter observations were useful in confirming that the radial crack system was always "well developed" (i.e., $c \geq 2a$; see Fig. 1)³² at failure, over the entire range of indentation loads used.

IV. Results

Figures 4 to 6 are plots of the inert strength vs indentation load results for the aluminas, barium titanates, and glass-ceramics, re-

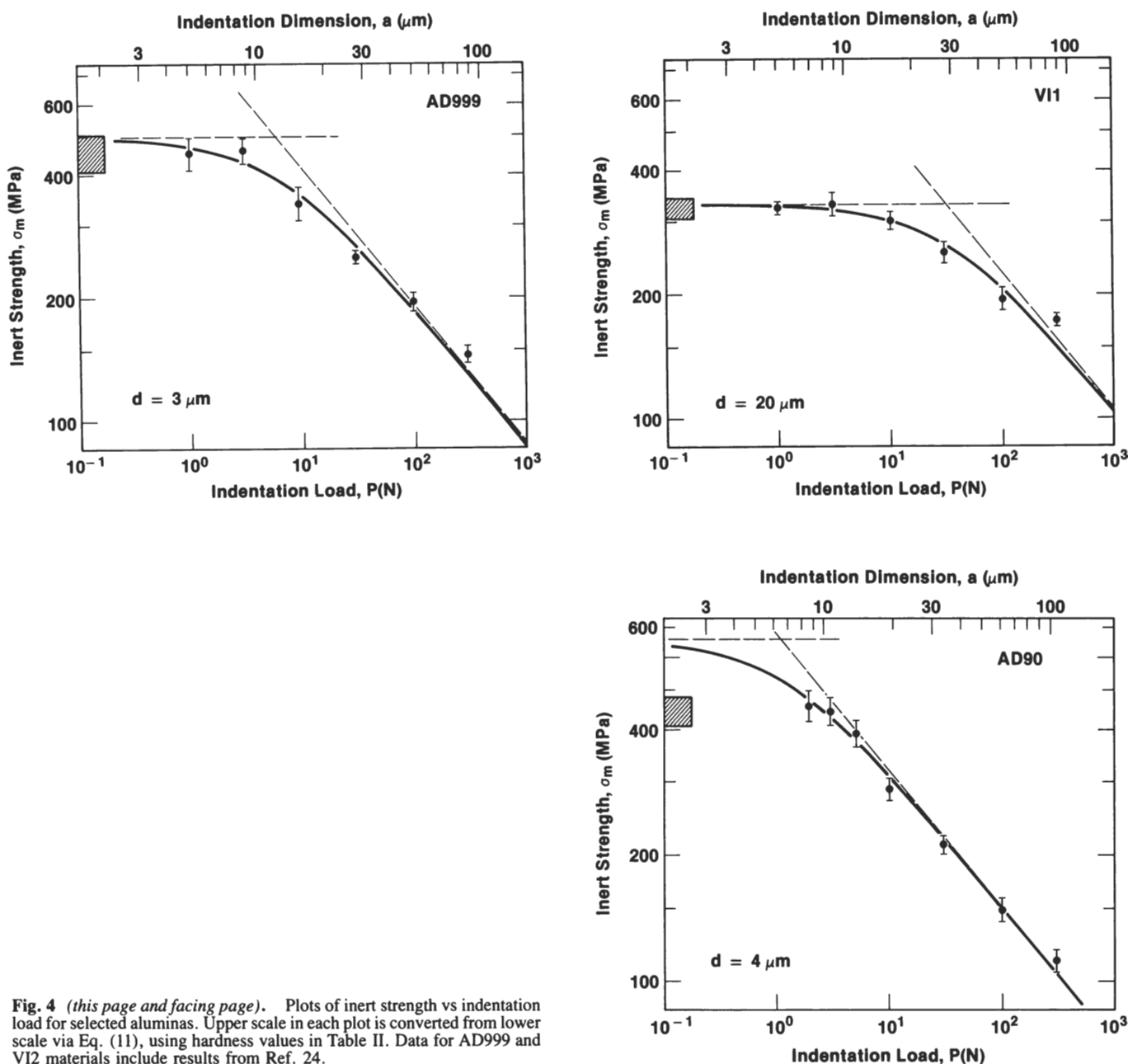


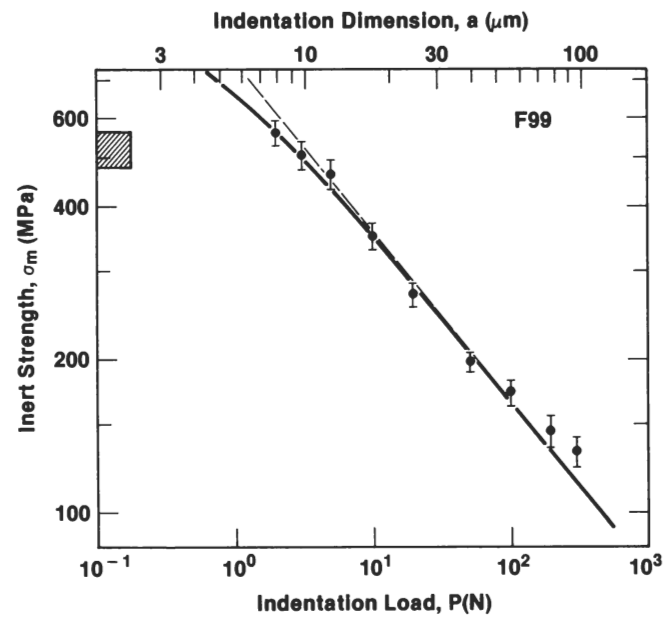
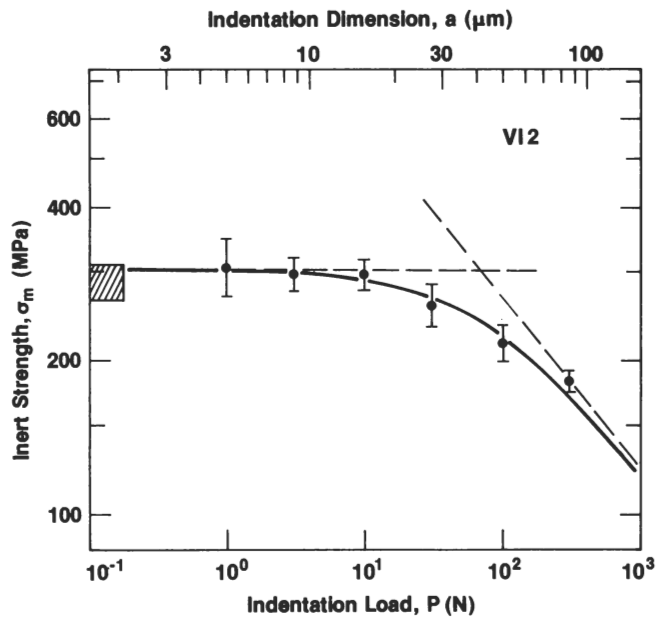
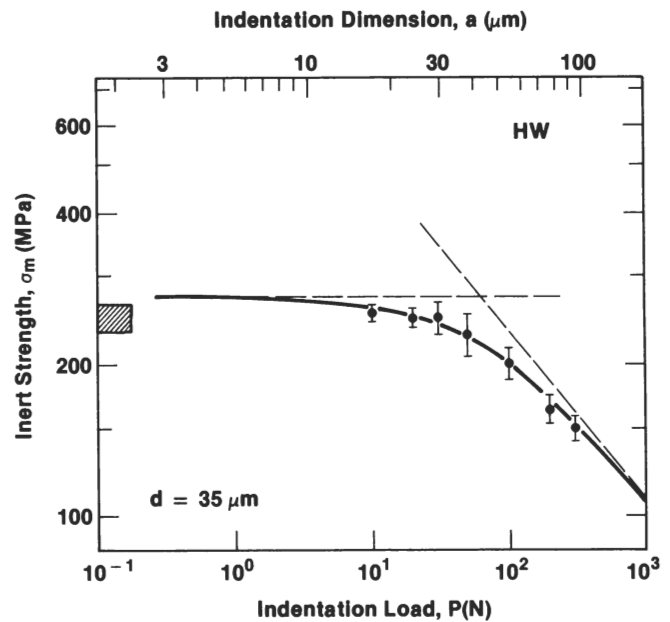
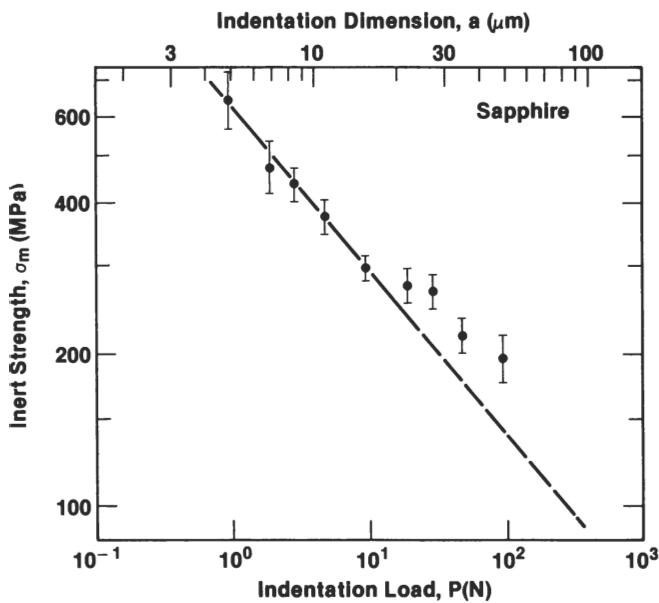
Fig. 4 (this page and facing page). Plots of inert strength vs indentation load for selected aluminas. Upper scale in each plot is converted from lower scale via Eq. (11), using hardness values in Table II. Data for AD999 and VI2 materials include results from Ref. 24.

spectively. Each data point represents the mean and standard deviation (evaluated in logarithmic coordinates) of 10 to 15 specimen breaks from indentation flaws at a prescribed load. The hatched region at the left of each plot represents a similar evaluation for breaks from natural flaws. The solid curves are least-squares best fits to the indentation data sets in accordance with Eq. (8) using σ_m^0 and $\sigma_m^0 P^{1/3}$ as adjustable parameters. These parameter adjustments define the asymptotic limits to the general strength function (i.e., corresponding to the solutions of Eq. (4)), as indicated by the broken lines in the plots. The values of σ_m^0 and $\sigma_m^0 P^{1/3}$ thus obtained, along with $P^* = (\sigma_m^0 P^{1/3} / \sigma_m^0)^3$ (see Eq. (8)), are listed in Table II. This table, which includes independently determined values of toughness and hardness, provides us with all the information that we need to quantify the microstructural effect for each material.

It will be noted in Figs. 4 to 6 that the tendency for the strength curves to "saturate" out at σ_m^0 in the low-load region is much stronger for some materials than others. This indicates considerable variability in the microstructural crack driving force term μQ in Eq. (3) (or equivalently, in χP^* in Eq. (5)), even within a

given class of materials. To show these intracomparisons more clearly, we have replotted the fitted curves for all materials within each group (in each instance covering only the load range used) onto "master" diagrams, Figs. 7 to 9. Special attention may be drawn to the fact that several of the curves intersect each other, particularly in the case of alumina (Fig. 7). It is therefore apparent that materials which show good strength characteristics at high loads do not necessarily do so at low loads. The dangers associated with unconditional extrapolation of data from macroscopic-crack tests into the practical domain of small-scale flaws are obvious.

An instructive way of demonstrating the universality of the R -curve behavior in the materials studied is to plot the results as K_c^{app} / K_c^∞ vs P / P^* according to Eq. (10), using $\sigma_m^0 P^{1/3}$ and P^* from Table II as normalizing parameters. Figures 10 to 12 are composite plots of this kind for the aluminas, barium titanates, and glass-ceramics, respectively. The theoretical prediction (solid curve from Fig. 3) fits the data points within the standard deviation error bounds (omitted here for clarity). This plotting scheme highlights the usefulness of P^* as a parameter for characterizing the degree of microstructural influence: those materials with large P^*



(most notably the VI aluminas in Fig. 10 and the NRL2 barium titanate in Fig. 11) plot way down on the curve, amounting to as much as a factor of 3 in apparent toughness reduction; those materials with small P^* barely deviate from the polycrystalline toughness plateau at the far right of the curve.

Let us now look more closely at the results in the asymptotically limiting regions of $P \gg P^*$ and $P \ll P^*$. The large P limit takes us into the conventional domain of continuum-based solutions, so we deal with it first. From Eq. (9) we see that the parameter $\sigma_m^P P^{1/3}$ appropriate to this domain relates to the polycrystalline toughness, K_c^P . Accordingly, plots of $\sigma_m^P P^{1/3}$ vs K_c^P (where data on the latter quantity are available, Table II) are shown in Figs. 13 and 14 for the aluminas and barium titanates. The straight lines in these figures are fits of slope $2/3$ in logarithmic coordinates, in line with the assumed constancy of ψ and χ in Eq. (9).[‡] The degree of

correlation observed here is not atypical of the general indentation toughness testing methodology.^{23,34}

The response at small P , if more complex, relates more closely to the microstructural effects of primary interest here. The first thing that may be noted is the tendency in many instances in Figs. 4 to 6 for the σ_m^0 asymptote to extrapolate to the unindented strength level. It would seem that the very same microstructural forces embodied in the K_m term in the indentation expression Eq. (3) are instrumental in determining the severity of the naturally occurring flaws. It follows as a corollary that the flaw populations in such instances are material intrinsic. On the other hand, there are several materials with relatively high σ_m^0 values for which the asymptotic extrapolations lie well above the unindented strengths. In these latter cases the inevitable intrusion of extrinsic failure origins, e.g., pores in the disk specimens and edge flaws in the bars, precluded extension of the data range into the plateau region.

The second point that draws attention in this plateau region is the apparent absence of any low-load cutoff response of the type indicated in Figs. 2 and 3. Such a cutoff, it will be recalled (Section II), has been proposed by some to occur when the flaws

[‡]Once again it is pointed out that this assumption may not always hold good. Strictly, the abscissa in Figs. 13 and 14 should contain a factor $(H/E)^{1/8}$, by virtue of the material dependence of χ .^{19,23} However, this is not a rapidly varying quantity within most groups of materials.

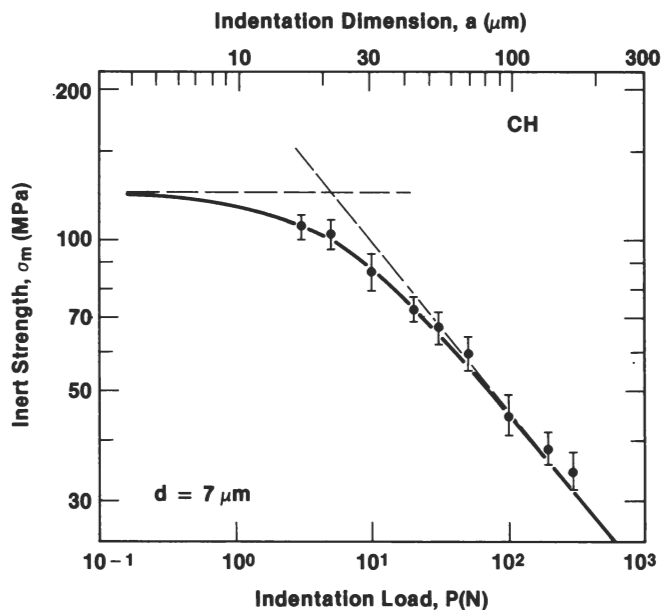
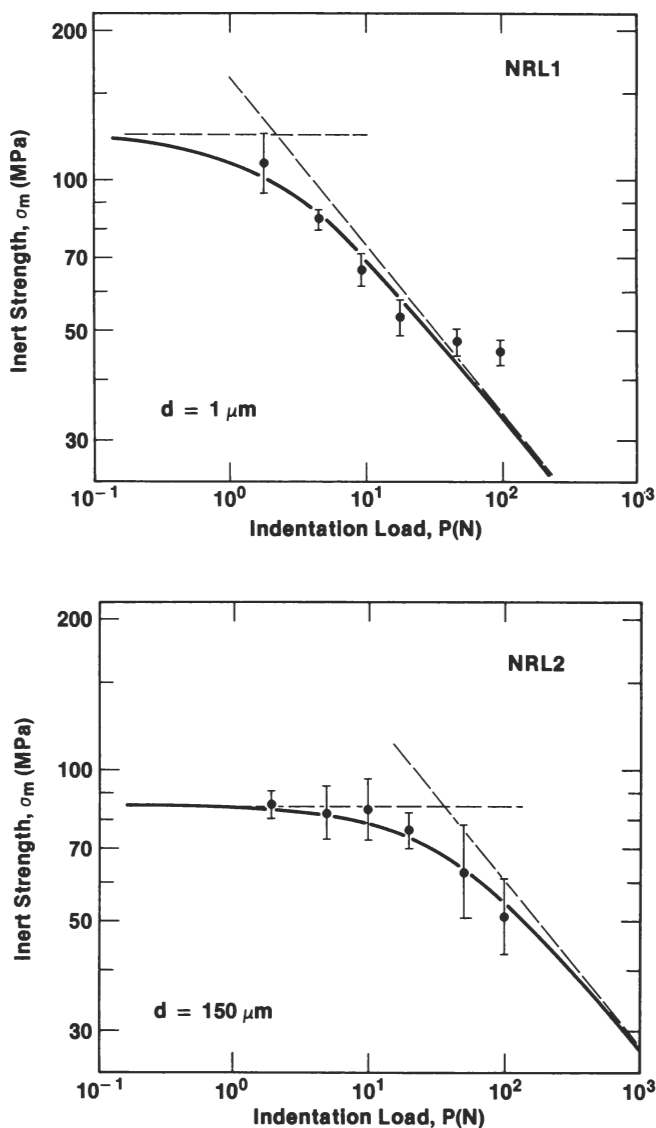


Fig. 5. Plots of inert strength vs indentation load for selected barium titanates (data for NRL materials courtesy of R. C. Pohanka).

Table II. Mechanical Parameters of Test Materials*

Material		σ_m^0 (MPa)	$\sigma_m^0 P^{1/3}$ (MPa \cdot N $^{1/3}$)	P^* (N)	K_c^* (MPa \cdot m $^{1/2}$)	H (GPa)
Al ₂ O ₃	Sapphire	0.7×10^6	660	0.08×10^{-9}	2.5	21.8
	AD999	488	883	5.9	3.9	20.1
	AD90	658	682	1.1	2.9	13.1
	VI1	329	1034	31.0		19.1
	VI2	302	1231	69.4	4.6	19.0
	F99	920	763	0.57		16.0
	HW	271	1083	63.8		17.0
BaTiO ₃	CH	124	215	5.2	1.05	5.2
	NRL1	123	160	2.2	0.84	
	NRL2	85	279	35.4	1.35	
Glass-ceramic	SL1	252	348	2.6		4.39
	SL2	257	406	3.9		4.27
	SL3	249	508	8.5		4.75
	VPI1	288	401	2.7		7.78
	VPI2	246	529	9.9		7.42
	VPI3	280	560	8.0		7.33

*Values obtained from independent large-crack techniques in these laboratories by S. M. Wiederhorn, D. B. Marshall, S. W. Freiman, and us.

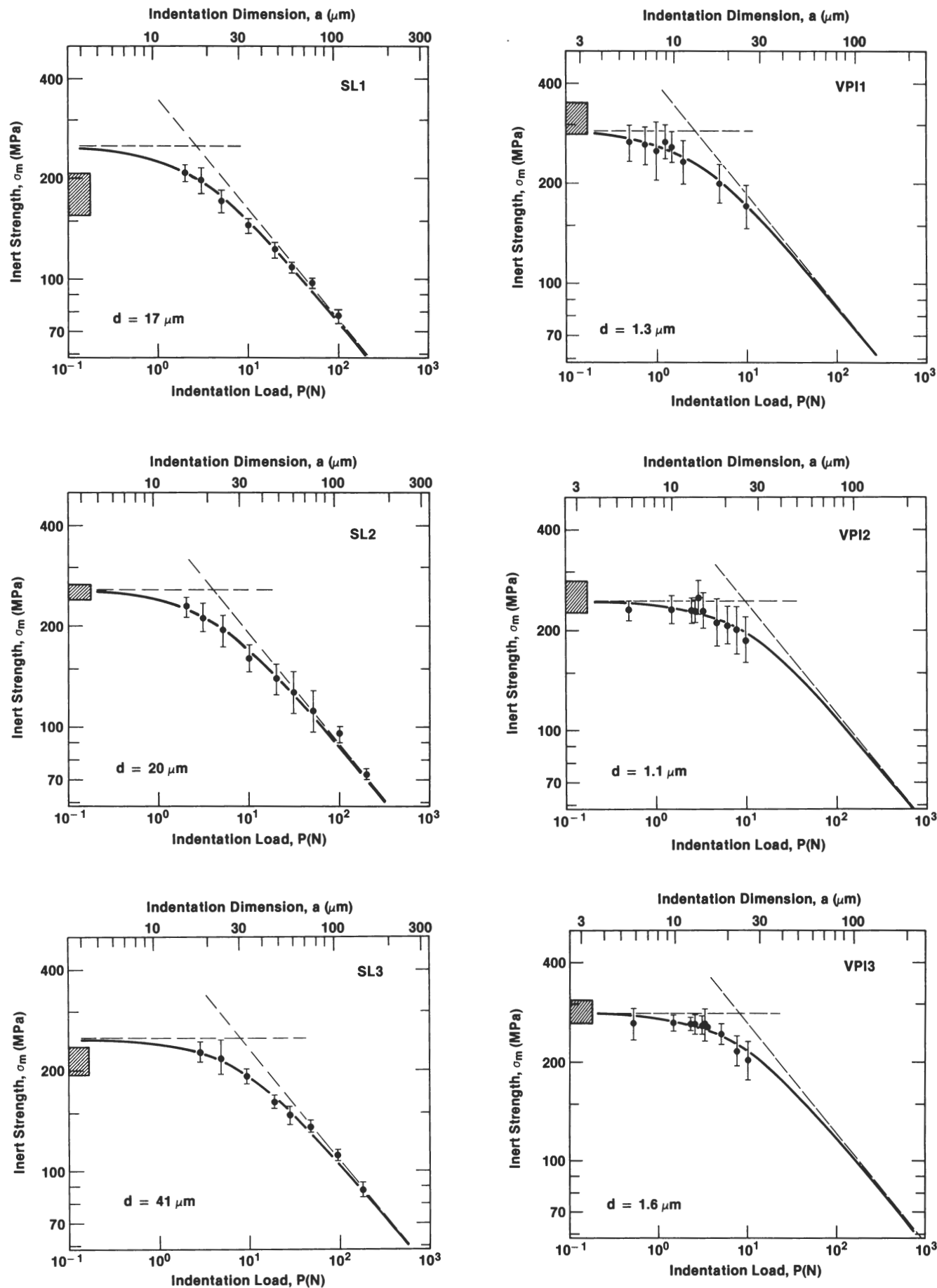


Fig. 6. Plots of inert strength vs indentation load for selected glass-ceramics; data for VPI materials reproduced from Ref. 25.

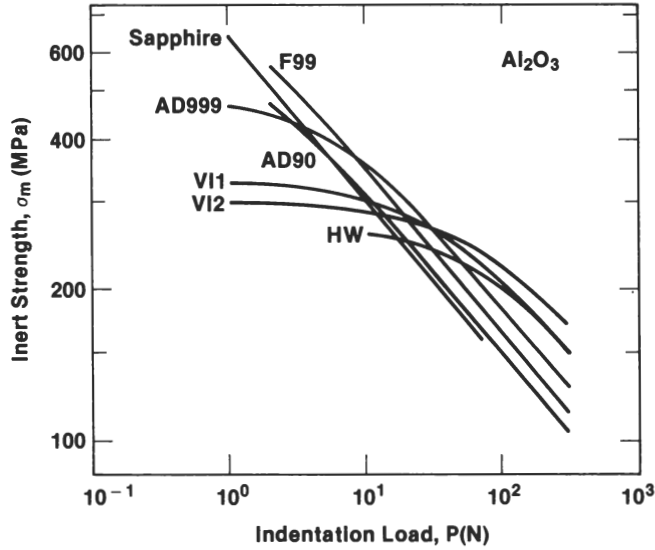


Fig. 7. Curves for aluminas from Fig. 4 replotted to produce master indentation-strength diagram.

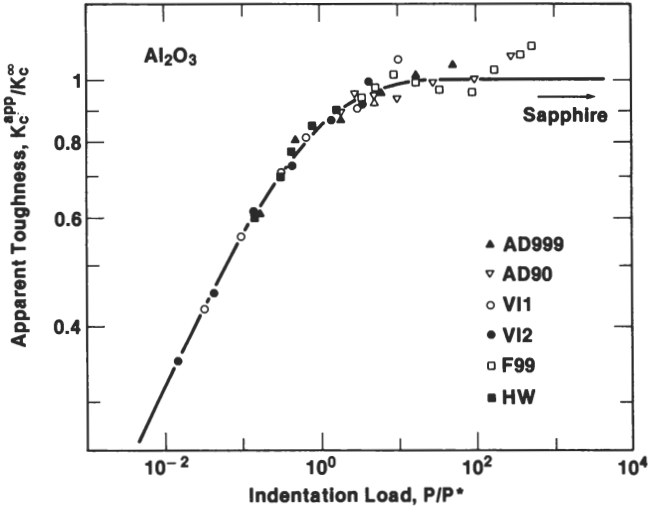


Fig. 10. Apparent toughness as function of indentation load for aluminas; data from Fig. 4 (error bars omitted), theoretical curve from Fig. 3.

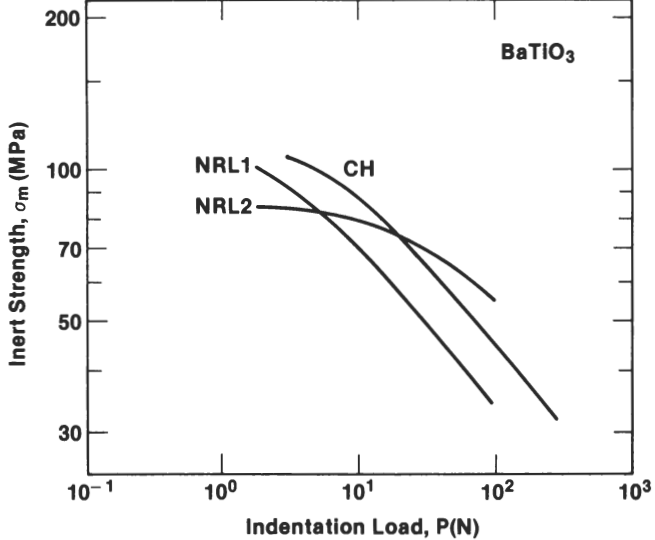


Fig. 8. Master indentation-strength diagram for barium titanates, replotted from fitted curves in Fig. 5.

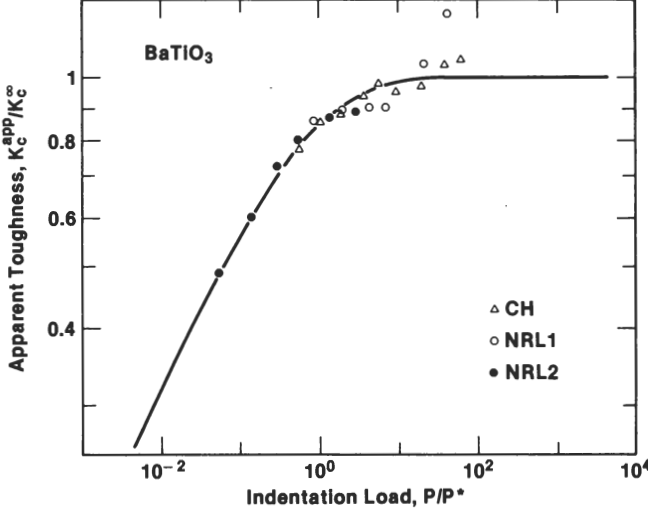


Fig. 11. Apparent toughness as function of indentation load for barium titanates; data from Fig. 5, theoretical curve from Fig. 3.

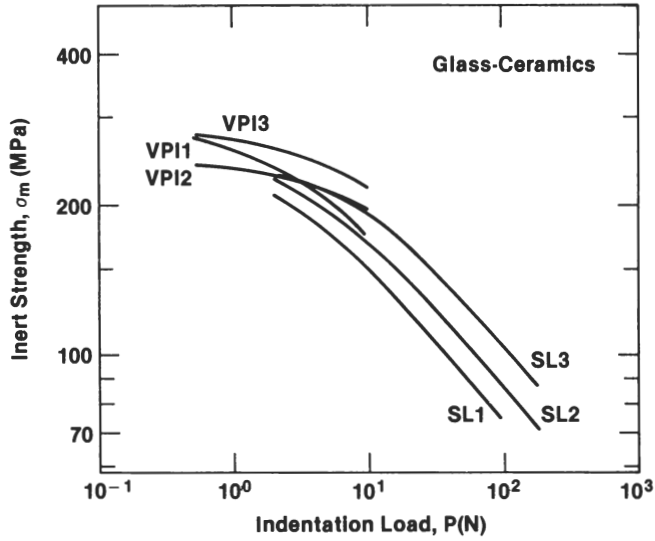


Fig. 9. Master indentation-strength diagram for glass-ceramics, replotted from fitted curves in Fig. 6.

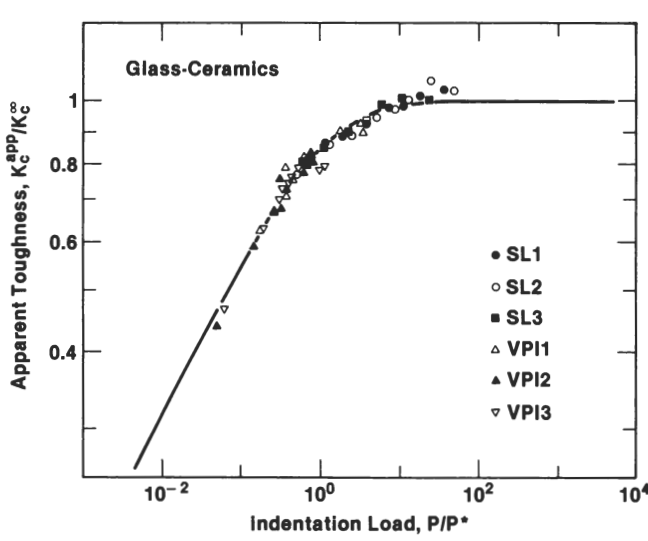


Fig. 12. Apparent toughness as function of indentation load for glass-ceramics; data from Fig. 6, theoretical curve from Fig. 3.

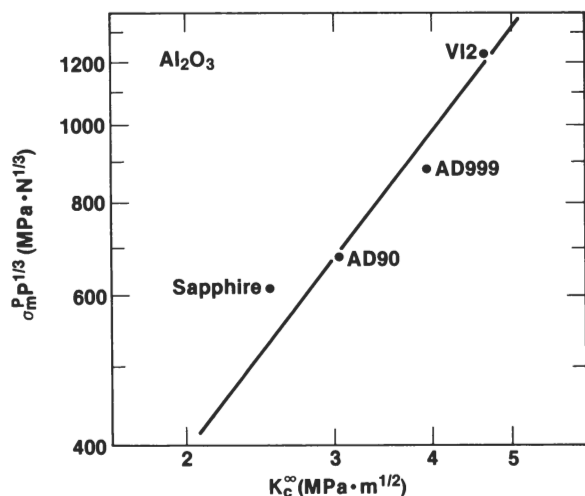


Fig. 13. Plot of $\sigma_m^p P^{1/3}$ vs K_c^∞ for aluminas, demonstrating correlation between indentation-strength data in large- P limiting region and macroscopic toughness values.

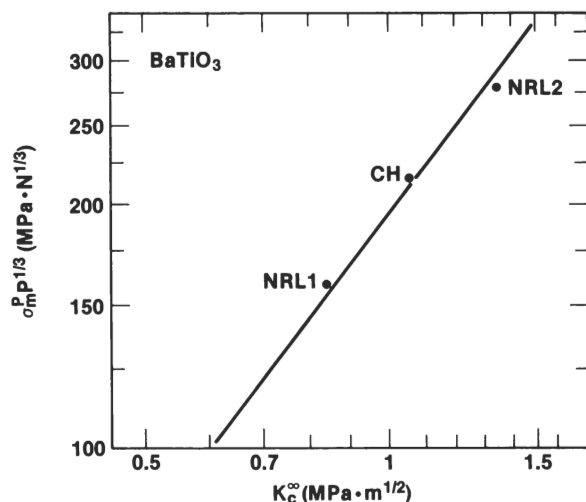


Fig. 14. Plot of $\sigma_m^p P^{1/3}$ vs K_c^∞ for barium titanates.

become so small as to be wholly encompassed within some controlling element of the microstructure. It could be argued that we are unlikely ever to be able to detect limiting behavior of this kind, owing to the increasing dominance of natural flaws (extrinsic or intrinsic) at lower P values (Section III). Nevertheless, there is one critical feature in the strength/indentation-load plots which is highly suggestive as to what may and what may not control the low-load response. This is the tendency in the master plot of Fig. 7 for the σ_m^0 plateau in the aluminas with the most pronounced R -curve behavior, particularly the VI grade materials, to cross well below the corresponding data line for sapphire. A measure of the scale of this crossover is that at the low end of the working load range in Fig. 7 the strength of sapphire is more than twice that of VI2 alumina. The implication here is that the small-scale fracture response is governed not by bulk cleavage properties, but rather by the energetics of some relatively weak grain interface. Unfortunately, the same assertion can not be made for the barium titanates and glass-ceramics in Figs. 8 and 9, for in those cases the appropriate single-crystal or matrix materials were unavailable to us to establish a reference data line. However, the fact that pronounced plateaus are as evident in these other material types as in aluminas would seem to suggest some commonality in the underlying microstructural driving forces.

It is in this context that the direct surface observations referred to in Section III proved especially useful. Generally, the indentation cracks in the materials studied did follow an intergranular path, although some transgranular fracture was observed in the initial extension from the impression corners. These characteristics were most readily seen in the VI2 grade alumina. Figure 15 is a typical example. Here the cracks begin their growth evolution in much the way as might be observed in sapphire,²³ but deflect immediately into the interfacial boundaries on reaching the extremities of the containing grains. In some cases the cracks re-emerged from the boundaries to pass through, rather than around, isolated grains. A similar interplay between intergranular and transgranular modes was noted by Smith and Pletka.³⁵ On applying an external tensile stress the cracks began to extend, tracing tortuous paths on the specimen surface, ultimately more than doubling their initial lengths. The picture that we arrive at is one of segmented crack propagation, averaging over the ultimate fracture surface such that the grain boundary becomes the controlling factor in the toughness.

To pursue this point concerning the inevitability of grain-boundary interaction one stage further, we may refer to the alternative, upper scale in Figs. 4 to 6, where we have plotted the

indentation dimension a using Eq. (11) (with H from Table II, where available). This dimension is about 1 order of magnitude smaller than the size of the critical radial crack, tip to tip, taking $2c_m \approx 5c_0 \approx 10a$ (Fig. 1). When account is taken of the values of the microstructural dimension d in Figs. 4 to 6, it is seen that the cracks must almost certainly intersect at least one boundary en-route to failure, even at the lowest indentation loads used.

Finally, the question may be raised as to which material parameters control the strength response in the low- P limiting region. Equation (4b) indicates that K_c^∞ remains a factor in the general accounting, but this is clearly not the key parameter. If it were, we would expect σ_m^0 to correlate well with $\sigma_m^p P^{1/3}$. We have already pointed out the lack of such correlation in the alumina master plot of Fig. 7, where the tendency for the curves to cross each other is pronounced. The next factor we might expect to have an important influence in Eq. (4b) is d , via Eq. (12). There is some indication from the progressively diminishing plateau levels for AD999, VII, VI2, and HW in Fig. 7 that the microstructural influence does increase with grain size. However, this still cannot be the whole story. The F99 alumina has a grain size intermediate between AD999 and VII (Table I), yet barely shows the beginnings of a low-load plateau. It could be argued that compositional additives must play some role in the microscopic fracture process, since of the five aluminas just mentioned F99 is the only one not specified as a "high-purity" material by the supplier. It is clear that we need to know more about the manner in which these compositional additives enter the host material, particularly at the grain interfaces.

V. Discussion

We have shown, using controlled indentation flaws, that the apparent toughness of ceramic materials can diminish dramatically as the scale of the fracture process reduces toward that of the microstructure. We have also shown that this kind of R -curve behavior can be accommodated within a simple fracture mechanics framework, by representing the microstructural crack driving force as a center load (real or effective) μQ on a pennylike crack system, in analogy to the center load χP associated with the residual indentation. As is evident from the fits to the strength data in Figs. 4 to 6, the theory provides a reasonable representation (i.e., within standard deviation error bounds) of the transition from microstructure-controlled failure at small c to indentation-controlled failure at large c . Thus we have, for the first time, a means of quantifying the microstructural influence on toughness in terms of routinely measurable experimental parameters; recall that

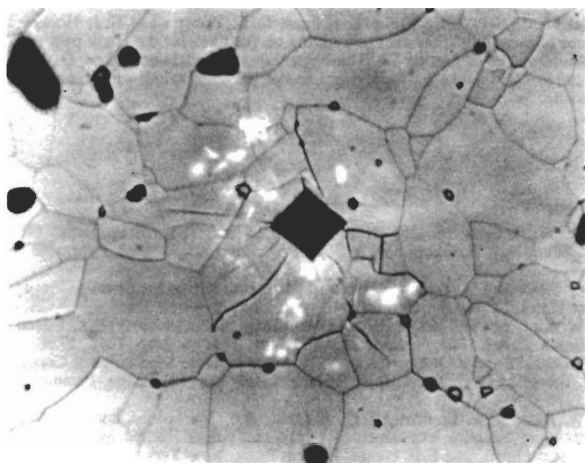


Fig. 15. Micrograph showing Vickers indentation ($P = 20$ N) in V12 alumina. Grain boundaries revealed by thermal etching prior to indentation. Note how radial cracks begin their initial growth evolution within individual crystal grains but tend thereafter to deflect into grain boundaries.

any two of the quantities σ_m^0 , $\sigma_m^0 P^{1/3}$, and P^* (Table II) are sufficient to specify the entire strength/indentation-load response for a given material.

To put all this into a proper perspective, it is important to identify those features which distinguish the present approach from the procedures adopted in the past. The first is the facility to control the size of the flaw, via the indentation load, so that the transition region between microscopic and macroscopic extremes may be explored in a systematic manner. This element of control is almost totally absent in postmortem fractographic methodologies^{3,36} where one is reliant on a widely distributed natural flaw population to map out the transition. Moreover, there are potential complications associated with crack geometry, residual stresses, etc., which tend to be overlooked in the failure analysis from natural flaws. The second feature is the amenability of the indentation system, by virtue of its well-defined configurational state, to explicit characterization in stress intensity notation. Attention may be drawn here to the way the center-loaded penny-crack representation referred to above allows us to set up Eq. (3) as a starting equation which can be solved in closed form, without in any way losing sight of the factors which make up the net fracture driving force. There are alternative treatments which reject this geometrical simplification in search of a superior indentation-load/crack-size function²⁵ (in analogy to our Eq. (7)); but these almost invariably contain an element of empiricism which tends to obscure the necessary physical bases for setting up any kind of strength analysis at all.

Some details of the microscopic-macroscopic transition behavior warrant further consideration here. It is convenient to begin at the large P end of the scale. We have seen that the strength-load parameter appropriate to this region, $\sigma_m^0 P^{1/3}$, scales with K_c^∞ (Figs. 13 and 14). The intimation is that the indentation testing approach, as embodied in such relations as Eq. (9), may be retained for evaluating conventional toughness properties, provided that we use only asymptotic data limits in these evaluations. Of course, all this is contingent on whether or not it is the macroscopic toughness that we *should* be interested in. It could be claimed that it is precisely the opposite end of the load scale which must determine the strength properties in most practical applications, for it is in this domain that natural flaw populations usually reside. Thus, as we progress down the R -curve in Figs. 10 to 12 we obtain toughness values which differ increasingly from those measured on large-crack specimens, but which at the same time become more representative of true flaw response.

Accordingly, let us turn our attention to the fracture mechanics formulation which allows us to describe the transition into this low-load domain. The key to the formulation is the $c^{-3/2}$ de-

pendence of the microstructural stress intensity factor K_m in Eq. (3). The validity of this functional dependence is reflected in the fits between the theoretical curves and experimental data in the strength plots of Figs. 4 to 6 and the “ R -curve” plots of Figs. 10 to 12. One might be justifiably surprised as to how good the fits appear to be in these plots, for two reasons. First, the value $-3/2$ for the exponent in the c dependence of K_m is contingent on the assumption that the microstructural force Q is localized at the crack center. Rice *et al.*⁷ have indicated that the net driving force is more properly evaluated in terms of the integrated contributions from all microstructural elements (grains, second-phase particles, etc.) intersected by the crack plane. The effect of such a distributed force configuration would be to increase the range of the microstructural influence, i.e., to reduce the magnitude of the negative crack-size exponent. In terms of the strength plot of Fig. 2, this increased range would be manifested as an extension of P^* further out along the load axis (accompanied, of course, by a flattening of the curve). However, even without this modification the value of P^* can be quite large. Taking the V12 alumina in Fig. 4 as an extreme example, $P^* = 69$ N or, equivalently, $a^* = 43$ μm ; together with the specification $d = 25$ μm for this alumina and our earlier assessment $\approx 10a$ for the critical crack size at failure (Section IV), we are talking about a range of influence of some 17 grain diameters in the region of microstructure-controlled fracture. This compares with the somewhat higher estimates of 50 to 100 grain diameters by Rice *et al.*⁷

The second reason for surprise is that our function $K_m(c)$ is continuous, yet we are dealing with materials which have discrete grain structures. The point can be made that effects of discreteness would tend to smooth out rapidly, since the number of grains traversed by the expanding radial crack front must increase in approximately quadratic manner with c . Nevertheless, the theoretical fits to the data appear to hold good down to the lowest loads achieved in Figs. 4 to 6. Special mention may be made in this context of the VPI glass-ceramic data in Fig. 6, where the smallest cracks are comparable to the crystallite size.²⁵ Here again, the stable crack extension during stressing to failure must have a smoothing effect. While on this subject of discreteness it may be pointed out that if one regards the high-load to low-load transition as abrupt (so that linear fits are made *through*, rather than *asymptotic to*, the data on either side of this transition), the conclusion may unjustifiably be drawn that the behavior is fundamentally inconsistent with $c^{-3/2}$ dependencies in the stress intensity factors.²⁵

Proceeding down the crack-size scale to the limit at low P , we find ourselves becoming involved in the issue of intergranular vs transgranular fracture. Unfortunately, the physical factors which control this competition are not well understood.³⁶ The evidence in this study, at least for the aluminas, suggests compellingly that it is the grain-boundary and not the bulk-crystal properties which hold the key to the strongest low-load turnovers in our strength curves (Fig. 7). In this interpretation, the K_m term in Eq. (3) is manifest as a progressive “weakening” of the boundary cohesion at diminishing crack sizes. Whether such weakening is associated with purely geometrical perturbations in the crack growth (in which case the K_m term in Eq. (3) should strictly be regarded as an effective, rather than real, driving force) or with internal microstresses is something that remains unanswered at this stage.²⁴ It would seem that a more fundamental investigation of grain-boundary structures is needed to resolve questions of this kind, and thence to explain why it is that the V12 alumina in Fig. 7 turns over so much more dramatically than the F99 alumina. The ultimate prospect is that one may be able to tailor ceramic interfaces so as to optimize the strength properties at all levels of crack size.

Having just made the case for the importance of grain-boundary structures, we should emphasize that materials which fracture transgranularly will not necessarily be immune to microstructural influences. There is nothing in either the geometrical perturbation or microstress processes which is exclusive to intergranular fracture. Indeed, there is some evidence that the larger grain-size barium titanates (e.g., NRL2, Fig. 8) do fail in a transgranular mode.³⁷ The implication from the present study is simply that the

strongest effects will be felt by those materials which have the weakest internal interfaces.

One of the conclusions drawn from our consideration of the strength data in Section IV was that the natural flaw distributions in materials with strong low-load turnovers tend to be structure intrinsic. The reason for this is that the microstructural driving force (K_m) has a stabilizing influence on crack growth. The most definitive indication of such an influence is the precursor growth stage in the strength tests. It is here that direct observations of indentations are especially valuable; a posteriori fractographic examinations of natural failure origins have not proved effective in detecting the existence of such a growth stage.

Finally, some comment is in order concerning the value of our method as a tool for characterizing microstructure-strength properties. It is well to remember that our fracture mechanics relation for the microstructural contribution to the crack driving force has a phenomenological ring to it. The treatment allows us to account for crack-grain scaling (R -curve) behavior without having to identify the underlying physical processes. This gives us readily measurable parameters (σ_m^0, P^*) for specifying the magnitude and range of the microstructural influence. From the standpoint of design, such parameters provide a scientific basis for extrapolating microscopic crack growth laws into the domain of natural flaws. Given that a particular material does exhibit strong plateau behavior at low indentation loads, the parameter σ_m^0 establishes an appropriate design strength; we then have a specification which, by the very nature of the stabilizing influences referred to in the previous paragraph, is insensitive to extraneous factors which might otherwise cause significant changes in the flaw population. Through the use of indentation flaws, this specification may be made with optimal simplicity, accuracy, economy, and unambiguity, thereby affording a sound rationale for materials-selection decisions.

VI. Conclusions

(i) Controlled indentation flaws constitute a powerful experimental methodology for the systematic study of microscopic-to-macroscopic (R -curve) crack-size effects in inert strength characteristics.

(ii) A fracture mechanics formulation, based on the assertion that the microstructural driving force for fracture may be regarded in terms of center-loaded penny-crack configurations (in direct analogy to the residual indentation driving force), fits the observed decline in "apparent" toughness on entering the domain of low contact loads.

(iii) This R -curve behavior can be specified explicitly in terms of a single additional quantity (σ_m^0 or P^*) over and above that needed to define the conventional macroscopic toughness response ($\sigma_m^p P^{1/3}$). It is suggested that these easily determined quantities should be useful as reliability parameters.

(iv) Different materials, even within a given class, can show great variability in toughness characteristics in the small crack-size region. Moreover, this variability is such that the inert-strength/indentation-load curves (e.g., Fig. 7) can cross each other, indicating the extreme danger of using toughness values from large-crack specimens to predict the response of natural flaws.

(v) For those materials with pronounced low-load plateaus in Figs. 4 to 6, the data fits extrapolate to the strengths levels for natural flaws. This shows that the same microstructural driving forces which act on the indentation flaws must also act on the natural flaws, implying that the populations in the latter case can be structure intrinsic.

(vi) The "range" of the microstructural influence can be substantial, extending in extreme cases (e.g., VI2) to well over 15 grain diameters.

(vii) The treatment presented here is formulated without commitment to specific physical processes. However, it is suggested that the indentation analysis should prove useful as a means for rationalizing the future study of these processes. Thus, for instance, the study of grain-boundary structures (notably in the aluminas) may be expected to provide valuable information on the sources of microstructure-controlled fracture.

Acknowledgments: The authors thank D. E. Roberts and B. J. Hockey for assistance in preparing specimens and setting up facilities for the crack path examinations referred to in Section III. Thanks are also due to T. L. Baker, D. Heuckeroth, and R. C. Pohanka for supplying some of the data included in Figs. 4 and 5, respectively.

References

- ¹S. M. Wiederhorn; pp. 217-41 in *Mechanical and Thermal Properties of Ceramics*. Edited by J. B. Wachtman, Jr. *Natl. Bur. Stand. (U.S.) Spec. Publ.*, No. 303 (1969).
- ²A. G. Evans and G. Tappin, "Effects of Microstructure on the Stress to Propagate Inherent Flaws," *Proc. Br. Ceram. Soc.*, No. 20, 275-97 (1972).
- ³R. W. Rice; pp. 323-45 in *Fracture Mechanics of Ceramics*, Vol. 1. Edited by R. C. Bradt, D. P. H. Hasselman, and F. F. Lange. Plenum, New York, 1974.
- ⁴S. Prochazka and R. J. Charles; pp. 579-98 in *Fracture Mechanics of Ceramics*, Vol. 2. Edited by R. C. Bradt, D. P. H. Hasselman, and F. F. Lange. Plenum, New York, 1974.
- ⁵R. W. Rice, S. W. Freiman, R. C. Pohanka, J. J. Mecholsky, and C. Cm. Wu; pp. 849-76 in *Fracture Mechanics of Ceramics*, Vol. 4. Edited by R. C. Bradt, D. P. H. Hasselman, and F. F. Lange. Plenum Press, New York, 1978.
- ⁶R. W. Rice, S. W. Freiman, and J. J. Mecholsky, Jr., "The Dependence of Strength-Controlling Fracture Energy on the Flaw-Size to Grain-Size Ratio," *J. Am. Ceram. Soc.*, 63 [3-4] 129-36 (1980).
- ⁷R. W. Rice, R. C. Pohanka, and W. J. McDonough, "Effect of Stresses from Thermal Expansion Anisotropy, Phase Transformations, and Second Phases on the Strength of Ceramics," *J. Am. Ceram. Soc.*, 63 [11-12] 703-10 (1980).
- ⁸R. W. Rice, S. W. Freiman, and P. F. Becher, "Grain-Size Dependence of Fracture Energy in Ceramics: I, Experiment," *J. Am. Ceram. Soc.*, 64 [6] 345-50 (1981).
- ⁹R. W. Rice and S. W. Freiman, "Grain-Size Dependence of Fracture Energy in Ceramics: II, A Model for Noncubic Materials," *J. Am. Ceram. Soc.*, 64 [6] 350-54 (1981).
- ¹⁰T. E. Adams, D. J. Landini, C. A. Schumacher, and R. C. Bradt, "Micro- and Macrocrack Growth in Alumina Refractories," *Am. Ceram. Soc. Bull.*, 60 [7] 730-35 (1981).
- ¹¹N. Claussen, B. Mussler, and M. V. Swain, "Grain-Size Dependence of Fracture Energy in Ceramics," *J. Am. Ceram. Soc.*, 65 [1] C-14-C-16 (1982).
- ¹²B. Mussler, M. V. Swain, and N. Claussen, "Dependence of Fracture Toughness of Alumina on Grain Size and Test Technique," *J. Am. Ceram. Soc.*, 65 [11] 566-72 (1982).
- ¹³B. J. Pletka and S. M. Wiederhorn, "A Comparison of Failure Predictions by Strength and Fracture Mechanics Techniques," *J. Mater. Sci.*, 17 [5] 1247-68 (1982).
- ¹⁴R. W. Rice and D. Lewis; pp. 659-76 in *Fracture Mechanics of Ceramics*, Vol. 5. Edited by R. C. Bradt, A. G. Evans, D. P. H. Hasselman, and F. F. Lange. Plenum, New York, 1983.
- ¹⁵A. G. Evans, "A Dimensional Analysis of the Grain-Size Dependence of Strength," *J. Am. Ceram. Soc.*, 63 [1-2] 115-16 (1980).
- ¹⁶A. V. Virkar, D. K. Shetty, and A. G. Evans, "Grain-Size Dependence of Strength," *J. Am. Ceram. Soc.*, 64 [3] C-56-C-57 (1981).
- ¹⁷D. B. Marshall and B. R. Lawn, "Residual Stress Effects in Sharp-Contact Cracking: I," *J. Mater. Sci.*, 14 [9] 2001-12 (1979).
- ¹⁸D. B. Marshall, B. R. Lawn, and P. Chantikul, "Residual Stress Effects in Sharp-Contact Cracking: II," *J. Mater. Sci.*, 14 [9] 2225-35 (1979).
- ¹⁹B. R. Lawn, A. G. Evans, and D. B. Marshall, "Elastic/Plastic Indentation Damage in Ceramics: The Median/Radial Crack System," *J. Am. Ceram. Soc.*, 63 [9-10] 574-81 (1980).
- ²⁰B. R. Lawn and D. B. Marshall; to be published in *Strength of Glass*. Edited by C. J. Kurkjian. Plenum, New York.
- ²¹B. R. Lawn and D. B. Marshall; to be published in *Fractography of Glass*. Edited by R. C. Bradt and R. E. Tressler. Plenum, New York.
- ²²T. F. Dabbs, B. R. Lawn, and P. L. Kelly, "A Dynamic Fatigue Study of Soda-Lime Silicate and Borosilicate Glasses Using Small-Scale Indentation Flaws," *Phys. Chem. Glasses*, 23 [2] 58-66 (1982).
- ²³P. Chantikul, G. R. Anstis, B. R. Lawn, and D. B. Marshall, "A Critical Evaluation of Indentation Techniques for Measuring Fracture Toughness: II, Strength Method," *J. Am. Ceram. Soc.*, 64 [9] 539-43 (1981).
- ²⁴B. R. Lawn, S. W. Freiman, T. L. Baker, D. D. Cobb, and A. C. Gonzalez, "Study of Microstructural Effects in the Strength of Alumina Using Controlled Flaws," *J. Am. Ceram. Soc.*, 67 [4] C-67-C-69 (1984).
- ²⁵R. Morena, K. Niihara, and D. P. H. Hasselman, "Effect of Crystallites on Surface Damage and Fracture Behavior of a Glass-Ceramic," *J. Am. Ceram. Soc.*, 66 [10] 673-82 (1983).
- ²⁶B. R. Lawn; pp. 1-25 in *Fracture Mechanics of Ceramics*, Vol. 5. Edited by R. C. Bradt, A. G. Evans, D. P. H. Hasselman, and F. F. Lange. Plenum, New York, 1983.
- ²⁷R. F. Cook, S. W. Freiman, B. R. Lawn, and R. C. Pohanka, "Fracture of Ferroelectric Ceramics," *Ferroelectrics*, 50 [1-4] 267-72 (1983).
- ²⁸R. F. Cook, S. W. Freiman, and T. L. Baker, "The Effect of Microstructure on Reliability Predictions for Glass Ceramics"; to be published in *Mater. Sci. Eng.*
- ²⁹R. C. Pohanka; unpublished work.
- ³⁰R. F. Cook, B. R. Lawn, T. P. Dabbs, and P. Chantikul, "Effect of Machining Damage on the Strength of a Glass-Ceramic," *J. Am. Ceram. Soc.*, 64 [9] C-121-C-122 (1981).
- ³¹D. B. Marshall, "An Improved Biaxial Flexure Test for Ceramics," *Am. Ceram. Soc. Bull.*, 59 [5] 551-53 (1980).
- ³²R. F. Cook, B. R. Lawn, and G. R. Anstis, "Fatigue Analysis of Brittle Materials Using Indentation Flaws: Case Study on a Glass-Ceramic," *J. Mater. Sci.*, 17 [4] 1108-16 (1982).
- ³³R. J. Roark; Ch. 7 in *Formulas for Stress and Strain*, 4th ed. McGraw-Hill, New York, 1965.
- ³⁴D. B. Marshall and B. R. Lawn; to be published in *Micro-Indentation Hardness Testing*. Edited by P. J. Blau and B. R. Lawn. *ASTM Spec. Publ.*, No. 899.
- ³⁵S. S. Smith and B. J. Pletka; pp. 189-209 in *Fracture Mechanics of Ceramics*, Vol. 6. Edited by R. C. Bradt, A. G. Evans, D. P. H. Hasselman, and F. F. Lange. Plenum, New York, 1983.
- ³⁶R. W. Rice; pp. 5-109 in *Fractography of Ceramic and Metal Failures*. Edited by J. J. Mecholsky and S. R. Powell. *ASTM Spec. Publ.*, No. 827 (1982).
- ³⁷R. C. Pohanka, R. W. Rice, and B. E. Walker, "Effect of Internal Stress on the Strength of BaTiO₃," *J. Am. Ceram. Soc.*, 59 [1-2] 71-74 (1976).